Hindawi
Advances in Materials Science and Engineering
Volume 2022, Article ID 2526281, 15 pages
https://doi.org/10.1155/2022/2526281

Research Article

Optimization of Mechanical Properties and Manufacturing Time through Experimental and Statistical Analysis of Process Parameters in Selective Laser Sintering

Adrian Korycki,[1,2] **Christian Garnier**,[1] **Valerie Nassiet**,[1] **Charles Tarek Sultan**,[2] **and France Chabert**[1]

[1]*LGP-ENIT-INPT, Université de Toulouse, 47 avenue d'Azereix, Tarbes 65016, France*
[2]*Prismadd, WeAre Group, 2 bis rue Georges Courteline, Montauban 82000, France*

Correspondence should be addressed to Christian Garnier; christian.garnier@enit.fr

Received 19 May 2021; Revised 27 January 2022; Accepted 9 February 2022; Published 29 April 2022

Academic Editor: Francesco Ruffino

A statistical analysis of the response of the parameters has been led by a design of experiments to extract the most influential parameters in the selective laser sintering process. The parametric study was carried out by varying five parameters on the SLS machine and by looking at their influence on five groups of responses relating to the physical, mechanical, and thermal properties as well as to the printing duration. The mathematical models of the response surfaces were established by linking the responses to factors and their interactions. The model of regression uses not only the interaction between regressors but also nonlinear logical functions. These statistical models were used to define an optimal set of parameters. The geometry and density of specimens made of polyamide 12 confirm that increasing the distance between successive laser beam passes allows a significant manufacturing time reduction. The mechanical properties depend mostly on laser power and scan count. We conclude that a low laser power applied twice can improve the properties of the printed part. By optimizing the laser parameters, the targeted mechanical properties are obtained with over 33% of production time savings.

1. Introduction

The selective laser sintering (SLS) process is an advanced manufacturing technology to print polymeric parts with high dimensional accuracy. The principle of SLS is to sweep a powder bed with a laser beam to melt the powder layer by layer. However, the printed parts suffer from mechanical resistance, which limits the printed parts as functional parts. Moreover, the printing cycle lasts a few hours, and consequently, the manufacturing costs are high. Improving the mechanical properties and reducing the manufacturing time are the key points of the widespread SLS process. Polyamide 12 (PA12) is the most used polymer in SLS. In order to improve the properties of the printed parts, it is necessary to obtain more information on the process parameters. From recent works [1–3], we know that the build parameters are as follows: supplied laser energy density and energy absorption, part bed orientation, feed and bed temperature, layer thickness and width, material type, and powder properties. These parameters can be classified into two categories: (a) part-dependent parameters and (b) build or layer parameters. Supplied laser energy and absorption and part orientation are part of the first group while preheating and processing temperature, heating rate from the preheating temperature to processing temperature, thickness and width of the sintered layer, material type, and its properties are part of the second one. The part-dependent parameters are different for each part in the build chamber, while the build or layer parameters (second category) can vary according to the height position of the part being processed into the build chamber. However, the build or layer parameters lead to the same properties within every single layer.

Several studies report an experimental investigation of the effect of parameters on the properties of sintered parts. The sintered structure is affected by the supplied laser energy density (ED). The energy density, also called Andrew number, is defined by the ratio of laser power over scan speed. The ED is known to impact the melting and solidification of the polymer, but above, each individual parameter, laser power, and scanning speed affect the properties of the printed parts for the same material. Sintering of polymers with low melting temperatures usually requires using CO_2 lasers with a wavelength of 10.6 μm. In the literature, the range of energy density for polyamide 12 is between 0.001 J.mm^{-2} and 0.048 J.mm^{-2} [4, 5]. The value below 0.01 J.mm^{-2} leads to not proper sintering, while the value above 0.048 J.mm^{-2} causes the degradation of the polymer. Caulfield et al. [6] reported that the parts fabricated at high energy density levels (0.028 J.mm^{-2}) have more ductile behaviour than PA12 samples made at low energy density levels (0.008 J.mm^{-2}). It has been found for Duraform PA12 (3D Systems) a maximum tensile strength of 48 MPa for horizontally printed samples and 44 MPa for vertically printed samples. According to the technical specification, the tensile strength of Duraform PA12 is 43 MPa. This leads to the conclusion that maximum strength can be obtained with a relatively low energy density. However, the elastic modulus has been reported at extremely low values of 1100 MPa for horizontal samples and 900 MPa for vertically printed samples. Nevertheless, Caulfield et al. [6] and Goodridge et al. [7] suggested that high laser power values may result in excess heat, which will result in damaged or burnt powder, shear stresses between layers, and part distortion. Khalil et al. [8] have also studied the influence of energy density in the range from 0.016 J.mm^{-2} to 0.032 J.mm^{-2} on flexural properties of ultra-high molecular weight polyethylene (UHMWPE). The elastic modulus and flexural stress increase with an increase in laser energy density. The maximum elastic modulus and flexural stress of 47 ± 3 MPa and 2.12 ± 0.05 MPa, respectively, are obtained for 0.027 J.mm^{-2}.

Some authors used response surface modelling (RMS) for the determination of the correlation between process parameters and part properties in SLS. Thus, Wegner and Witt [9] studied the effect of the laser power, scan spacing, scan speed, preheating temperature, and layer thickness on the tensile strength, tensile modulus, elongation at break, and part density of polyamide parts (PA 2200 from EOS). They reported that the most important parameters are the scan spacing and layer thickness. Negi et al. [10] investigated the effect of process parameters as preheating temperature, laser power, scan speed, and scan spacing on the properties such as tensile strength, elongation, yield strength, and tensile modulus of glass-filled polyamide parts (PA 3200 GF from EOS) produced by SLS. Several authors [6, 9–12] confirm that the mechanical properties of sintered parts increase with an increase of laser power and preheating temperature and decrease with an increase in scan speed and scan spacing. The scan speed and scan spacing are found to have a positive effect on the properties, while the preheating temperature and laser power have a relatively small influence on the properties. Moreover, Ajoku et al. [13] found that, for PA12 (no material reference is cited in this work), better properties of tensile strength, Young's modulus, and elongation at break are obtained with a part build orientation parallel to the layer orientation (0°) than for parts built perpendicularly to layer orientation (90°). To sum up, the experimental studies are time-consuming, and the parameters cannot be separated to understand their effect because they are interdependent.

To facilitate the analyses, different process parameters in SLS are often correlated with part properties by applying the design of experiments (DoE). This approach is used to plan the experiments, and regression models can be developed to study the effect of selected parameters, including their interactions concerning output. Hofland et al. [14] present the study for polyamide 12 (PA 2200 from EOS), using the sensitivity analysis, considering laser power, scan speed, scan spacing, part build orientation, preheating temperature, and layer thickness. They have shown that the most important variable is scan spacing, with a result of 30% and 23% for horizontal and vertical printed samples, respectively. Next, the layer thickness of 29% for horizontal printed samples and 28% for vertical printed samples were obtained from calculations. Scan speed led to the third-largest impact on the part properties, followed by preheating temperature and laser power. Kumar et al. [2] have analysed the influence of laser power, temperature, and part orientation for the dimensional accuracy and microhardness of parts. They conducted their experiments using the Taguchi method for the L_9 orthogonal array setting with Duraform PA (3D Systems). The Taguchi technique can be successfully used to optimize and investigate the effect of parameters over the variables. They confirm that laser power and temperature have a major influence over the dimensional accuracy; moreover, the temperature has an important influence on the microhardness of the SLS prototypes. Another method of design of experiments is response surface modelling. This method was used by Wegner and Witt [9] or Negi et al. [10]. They both have designed orthogonal and rotatable, Wegner and Witt studied 36 experiments, and Negi used 50 experiments. In orthogonal designs, the coefficients are independent of each other, resulting in a simpler interpretation of the data. Rotatable designs have experimental variances which are equal for all points with the same distance from the centre point, being independent of the chosen direction. Yusoff and Thomas [15] have justified that the laser energy density depends on three variables, laser power, scan count, and laser scan spacing, for Duraform PA (3D Systems) and PA 2200 (EOS). The latter plays a significant role in experimental results. According to Stwora and Skrabalak [16], the scanning speed does not influence the properties of the part. However, maximizing scan speed might reduce the manufacturing time in the case of building large elements.

Most of the time, several parts are manufactured at the same time in the same build chamber for powder savings. During one manufacturing cycle, the parameters can be chosen for each individual part. Many parameters affect the properties of the printed parts, so the studies aiming to understand the effect of parameters take a long time, and they are expensive. Moreover, understanding the effect of

each parameter is tricky since the parameters are interdependent. To understand the effect of process parameters, the use of mathematical methods such as the design of experiments is required. Shen et al. [17] have proposed experimental testing and numerical modelling to evaluate and predict the temperature distribution and dimensions of their melt pools. Their model takes into account the interaction between the laser beam and powder bed, as well as the temperature-dependent material properties and the solid-liquid phase transition. The process modelling can provide an insight into the mechanism of the sintering process by heat transfer model and heat source modelling. The process parameters for SLS of the nanocomposite powders are optimized through the process efficiency maps. Korycki et al. [18] also studied a combined experimental-numerical approach to estimate the influence of each thermal cycle on the crystallinity and the mechanical properties of the printed layers during SLS. A dual experimental-theoretical method has been investigated by Yuan et al. [19] on multiwalled carbon nanotubes coated polyamide 12 (CNTs/PA12) powders. The energy required for melting and decomposition was predicted by a theoretical model after the implementation of characterized heat capacity and density in the powder, melting, and liquid phases. It is noted that this method of material evaluation and process optimization is cost-effective. Another method proposed to save optimization time and manufacturing costs is the adaptive network-based fuzzy inference system (ANFIS) studied by Aldahash et al. [20] for cement-filled polyamide 12 composite. It is an iterative tool for optimizing nonlinear and multivariable manufacturing operations. For this study, a set of cement-filled PA12 test specimens was manufactured by SLS with 8 different values of laser power (4.5–8 W) and 8 different weight fractions of white cement (5–40%). ANFIS is used for the prediction of chaotic time series, where the goal is to minimize the prediction error.

We propose the iconography of correlation (CORICO) as a method [21, 22] to help to get insight into the effect of process parameters. It is an extension of interactions of partial correlation as a factor selection tool and synthetic diagram including the chosen factors. Figure 1 shows an example in the case of corrosion study for which the factors are concentration, temperature, and time. This method allows the screening of factors and the construction of nonlinear models by a study of interactions such as concentration and temperature, as shown in Figure 1. The responses are expressed as multiple regressions. In the CORICO method, the selection of predictors takes place before the model is fitted and the calculation of coefficients is performed. The number of variables is unlimited, and the CORICO method proposes the model which fits the best with the experimental data. To our knowledge, it is the first time that the iconography of the correlation method is applied to parts manufactured in the selective laser sintering process.

For this study, in experimental analysis, 400 specimens of Duraform FR1200 have been sintered on the ProX500 SLS. The specimens have been characterized to measure their density, porosity, flexural and tensile properties, and thermal transitions. Also, the manufacturing time has been measured for each specimen. To our knowledge, it is the first time that the production time of sintered parts is included in such a study.

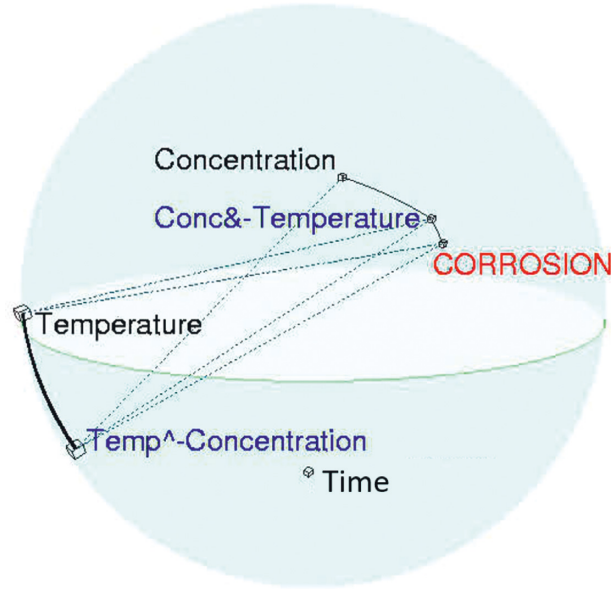

Figure 1: CORICO software: global data analysis.

In this work, the level of input of each parameter has been chosen following the recommendation of the supplier of the machine and powder. However, the parameters can be applied as well on the others SLS machines and powders. We target the best performance for the printed parts. Therefore, the influence of the different parameter settings on density, thermal transitions, and mechanical properties of laser-sintered polyamide 12 parts is analysed.

In the second part of this work, the iconography of correlations method as statistical analysis allows optimizing the process parameters in order to improve the mechanical properties and to decrease the production time of printed parts.

2. Materials and Methods

2.1. Materials. Sintered material was polyamide 12, under the commercial name of Duraform FR1200 from 3D Systems, with a melting temperature of 180°C. The sintered part density is about 1.02 g.cm^{-3}. Duraform FR1200 is characterized by flame retardant with excellent surface quality for applications such as aerospace, transportation, and consumer goods. The safe level of smoke density and toxicity allows introducing direct 3D production in aerospace to accelerate parts delivery and reduce downtime.

The sintering experiments were carried out by using a commercial ProX500 SLS machine from 3D Systems, equipped with a CO_2 laser of 500 microns diameter beam size, which allows sintering of specimens with a maximum

power of 100 W and maximum laser scanning speed of 12000 mm.s^{-1}. The scan count can be once or twice. The maximum scan spacing is 0.25 mm.

2.2. Experimental Methods. The Archimedes principle [23] was used to determine bulk density ρ_{bulk} by hydrostatic weight. This method can measure the density of the entire part considering its porosity. The measurement procedure for the hydrostatic density of the sintered part is as follows:

(i) Drying at least 3 h at 100°C

(ii) Weight of dried sample in the air (M_1)

(iii) Weight of water-saturated sample in water (M_2) at 27°C, while the density of water (ρ) is 0.9965 g.cm^{-3}

The determined M_1, M_2, and ρ are substituted in equation (1). The bulk density is obtained in g.cm^{-3}.

$$\rho_{bulk} = \frac{M_1}{M_1 - M_2} \times \rho_{H_2O}. \quad (1)$$

The relative density in equation (2) includes porosity. It is calculated by the ratio of bulk density ρ_{bulk} and theoretical density of fresh powder ρ_{true} (1.095 g.cm^{-3}, measured by pycnometer in ethanol).

$$\rho_{relative} = \frac{\rho_{bulk}}{\rho_{true}} \times 100\,\%. \quad (2)$$

The dimensional control of specimens is done according to ISO 2768. A medium tolerance class is applied to linear dimensions of sintered parts. Three individual measurements (length, thickness, and width) of each dimension are taken, and an average value is obtained. The dimensions are measured using Vernier calliper with an accuracy of 0.1 mm, while the length of tensile samples is measured by a ruler with an accuracy of 0.1 mm. The results are compared to the dimensions of the input drawing.

The linear shrinkage of sintered parts is calculated as follows:

$$\begin{aligned} L_{shrinkage} &= \frac{(L_0 - L)}{L_0}\ [\%], \\ W_{shrinkage} &= \frac{(W_0 - W)}{W_0}\ [\%], \\ T_{shrinkage} &= \frac{(T_0 - T)}{T_0}\ [\%], \\ V_{shrinkage} &= \frac{(V_0 - V)}{V_0}\ [\%], \end{aligned} \quad (3)$$

where L_0 (length), W_0 (width), and T_0 (thickness) are the nominal size of the printed parts, L, W, and T are the actual size of length, width, and thickness (mm), respectively, and V_0 and V are the nominal and actual volume of the printed parts (mm^3).

The mechanical tests are carried out on the Instron Universal 33R4204 traction machine. The tests are performed on flexural specimens by three-point bending tests according to ISO 178. The flexural samples are designed with a nominal dimension of 127 mm, 12.7 mm, and 3.2 mm corresponding to long, wide, and thick, respectively. The tensile specimens are prepared according to ISO 20753 (types and dimensions), and their properties are determined by ISO 527. The samples are designed with a nominal dimension of 170 mm, 10 mm, and 4 mm corresponding to long, wide, and thick, respectively. The test parameters are as follows: movement speed of 2 mm.min^{-1}, 5 kN force cell, span length of 56 mm for flexural specimens only, and Instron 2620 series extensometer for tensile specimens only, and end of the test criterion is the rupture of the test specimen.

The thermal transitions are measured with DSC Q200 from Thermal Analysis Instruments. The measurements are performed under nitrogen sweep at 50 ml.min^{-1} and heating and cooling rates of 15°C.min^{-1} from room temperature to 300°C. A sample mass between 8 mg and 16 mg is placed in an aluminium hermetic crucible. The glass transition temperature (T_g), crystallization temperature (T_c), and melting temperature (T_m) are determined. The apparent degree of crystallization (X_c) is calculated with the following formula:

$$X_c = \frac{\Delta H_m}{\Delta H_{th}} \times 100\,\%, \quad (4)$$

where ΔH_m is the melting enthalpy and ΔH_{th} is the theoretical melting enthalpy of 100% crystalline phase equals 209.3 J.g^{-1} for PA12 of 100% crystalline phase [24].

The production time in seconds is calculated to obtain the time needed to print a single sample for a set of parameters.

$$t_p = \left(\frac{T}{SS} L \frac{SC_f}{LS_f} + (2T + 2L)\frac{SC_o}{LS_o}\frac{W}{LPT}\right) + 2\frac{T}{SS} L \frac{SC_o}{LS_o}, \quad (5)$$

where T is the actual thickness (mm), L is the actual length (mm), W is the actual width (mm), LPT is the layer thickness (mm), SS is the laser scan spacing (mm), SC_f is the fill scan count, LS_f is the fill laser beam speed (mm.s^{-1}), SC_o is the outline scan count, and LS_o is the outline laser beam speed (mm.s^{-1}).

2.3. Statistical Method

2.3.1. Iconography of Correlation. The empirical models for mechanical properties and the influence of selected parameters were studied. The models were developed by the design of experiments based on energy density. The selected combinations consist of factors at two, three, and five levels. The design of experiments is analysed by using the iconography of correlations method named CORICO and discussed per output response.

The correlation coefficient allows the comparison of deviations around the mean of two variables x and y, and the mathematical evaluation distinguishes their variations [25]. The variation of each variable can be represented by a vector represented in n-dimensional space. The correlation coefficient is the cosine (in a space with n dimensions) of the angle that differentiates the "deviation vectors" X and Y, whose respective coordinates are X_i and Y_i:

$$r(x,\ y) = \cos(X,Y) = \frac{X_1Y_1 + X_2Y_2 + \ldots + X_nY_n}{\sqrt{X_1^2 + X_2^2 + \ldots + X_n^2}\sqrt{Y_1^2 + Y_2^2 + \ldots + Y_n^2}}. \quad (6)$$

The CORICO method relies on the calculation of total and partial correlations. Each observation pair corresponds to one moment and only one. If the vectors are collinear, the cosine is equal to 1. If the two vectors are orthogonal, the cosine is equal to 0.

2.3.2. Design of Experiments. Based on the literature, the process parameters, such as fill laser power, fill scan count, outline laser power, outline scan count, and scan spacing, are selected due to their dominant influence on sintered part quality. These process parameters are defined as follows:

(i) Laser power, the amount of power or energy available from the laser beam.

(ii) Scan count, the number of rescan passes for laser movements on the surface of part.

(iii) Scan spacing, the distance between two neighbouring parallel scan lines.

The ranges of factors were optimized based on energy density [26]. The fill and outline energy density ED in J.mm^{-2} that affect the part quality have been calculated according to the following equation:

$$\mathrm{ED} = \frac{\mathrm{LP} \times \mathrm{SC}}{\mathrm{SS} \times \mathrm{LS}}, \quad (7)$$

where LP is the laser power (W), SC is the scan count, SS is the laser scan spacing (mm), and LS is the laser beam speed (mm.s^{-1}). The standard print mode is characterized by a scanning strategy "fill and outline" option. With our printing SLS machine, the laser beam can scan the entire cross-section with 12000 mm.s^{-1} speed and the contour with a speed of 3500 mm.s^{-1}.

The energy density for polyamide 12 was kept between 0.01 J.mm^{-2} and 0.048 J.mm^{-2} [27]. The experiments were executed at five independent input variables, which were varied up to five levels in the range of parameters available in the machine. Different process parameters and their values, which have been optimized through the experimental study, are presented in Table 1. The rest of the parameters, such as fill scan speed, outline scan speed, temperature, and powder layer, were kept constant.

The laser power has been chosen at a maximum of 45 W to limit the possibility of material degradation. Scan count was defined at 1 or 2 to be sure to give enough energy to melt the material without significantly affecting the production time. Finally, scan spacing from 0.15 mm to 0.25 mm corresponds to the overlap, which has been defined from 30% to 50% of the beam diameter in order to melt the material to a greater or lesser extent and thus to act on the cohesion between two adjacent lines.

Any design of experiment allows characterizing not only the factors and their influences but also the desired answers. As the development of parameter sets on the used SLS machine is required, the answers concern the mechanical and geometrical characteristics of printed parts. Production time is investigated to reduce the manufacturing time and costs.

Table 1: Process parameters and their values.

Process parameters	Studied parameters				
	1	2	3	4	5
Fill laser power, LPf (W)	15	20	30	40	45
Fill scan count, SCf [-]	1	2			
Outline laser power, LPo (W)	10	13	15	—	—
Outline scan count, SCo [-]	1	2			
Scan spacing, SS (mm)	0.15	0.20	0.25	—	—

The forty sets of parameters presented in Table 2 have been selected according to the range of energy density to obtain proper sintering parts without degradation. The inert gas atmosphere of nitrogen has been used during the sintering process to prevent polymer degradation. The tests were performed for the fixed preheating temperature of 130°C, part bed temperature of 173°C, and powder layer of 0.1 mm. Experiment N°9 corresponds to processing parameters recommended by the supplier 3D Systems: fill laser power of 2×20 W, outline laser power of 2×10 W, and scan spacing of 0.20 mm proposed by the supplier of machine and powder (3D Systems).

Five tensile specimens and five flexural specimens were manufactured in *YZ* axis *Y* orientation. Their length is parallel to the *Y*-axis, width parallel to the *Z*-axis, and thickness parallel to the *X*-axis. Figure 2(a) shows the geometry and dimensions of the specimen. The laser pass, which is perpendicular to the specimen length, is drawn in the same figure; the red lines represent laser passes. Firstly, a contour line (outline) with a 90° rotation sinters the outline of the specimen for each layer, and then, parallel laser lines fill the inner specimen (inline). The sintered parts were fabricated following standards for comparison of their properties. The printed specimens are displayed in Figure 2(b).

The models of regression were developed by analysing the measured data with the CORICO method. The effects of significant variables and potential interactions were estimated on the studied answers. In the models, the different terms are ranked by decreasing importance, each of them explaining the residue not explained by the preceding ones.

In order to optimize the set of parameters, the models of regression can be used to minimize or maximize the response (Monte Carlo method). The results may be subjected to one or more validation tests which, integrated with the previous results, will refine the model.

3. Results and Discussion

3.1. Experimental Analysis

3.1.1. Density and Porosity. The powder particles are sintered by the heat of the laser beam, and therefore, the part density and porosity depend on the energy density provided by the laser [28]. The sintered parts have achieved bulk

Table 2: Experimental design with variable values for Duraform FR1200.

Exp. N°	Fill laser power (W)	Fill scan count [-]	Outline laser power (W)	Outline scan count [-]	Scan spacing (mm)	Fill energy density ($J.mm^{-2}$)	Outline energy density ($J.mm^{-2}$)
1	15	2	10	2	0.15	0.017	0.038
2	15	2	10	1	0.15	0.017	0.019
3	15	2	13	1	0.15	0.017	0.025
4	15	2	15	1	0.15	0.017	0.029
5	20	2	10	2	0.15	0.022	0.038
6	20	2	10	1	0.15	0.022	0.019
7	20	2	13	1	0.15	0.022	0.025
8	20	2	15	1	0.15	0.022	0.029
9	20	2	10	2	0.20	0.017	0.029
10	20	2	13	2	0.20	0.017	0.037
11	20	2	13	1	0.20	0.017	0.019
12	20	2	15	2	0.20	0.017	0.043
13	20	2	15	1	0.20	0.017	0.021
14	30	1	10	2	0.15	0.017	0.038
15	30	1	10	1	0.15	0.017	0.019
16	30	1	13	1	0.15	0.017	0.025
17	30	1	15	1	0.15	0.017	0.029
18	40	1	10	2	0.15	0.022	0.038
19	40	1	10	1	0.15	0.022	0.019
20	40	1	13	1	0.15	0.022	0.025
21	40	1	15	1	0.15	0.022	0.029
22	40	1	10	2	0.20	0.017	0.029
23	40	1	13	2	0.20	0.017	0.037
24	40	1	13	1	0.20	0.017	0.019
25	40	1	15	2	0.20	0.017	0.043
26	40	1	15	1	0.20	0.017	0.021
27	45	1	10	2	0.15	0.025	0.038
28	45	1	10	1	0.15	0.025	0.019
29	45	1	13	1	0.15	0.025	0.025
30	45	1	15	1	0.15	0.025	0.029
31	45	1	10	2	0.20	0.019	0.029
32	45	1	13	2	0.20	0.019	0.037
33	45	1	13	1	0.20	0.019	0.019
34	45	1	15	2	0.20	0.019	0.043
35	45	1	15	1	0.20	0.019	0.021
36	45	1	10	2	0.25	0.015	0.023
37	45	1	13	2	0.25	0.015	0.030
38	45	1	13	1	0.25	0.015	0.015
39	45	1	15	2	0.25	0.015	0.034
40	45	1	15	1	0.25	0.015	0.017

hydrostatic density in the range from $1.006\,g.cm^{-3}$ to $1.036\,g.cm^{-3}$. The highest density was obtained for exp. N°13, while the lowest density had exp. N°38. We target the highest density since a high porosity rate means poor mechanical resistance. Very close to our results, Wegner and Witt [9] have reported the density of PA12 approximately at $0.998\,g.cm^{-3}$, while Caulfield et al. [6] found higher values of $1.050\,g.cm^{-3}$ for horizontally printed specimens. According to the datasheet of Duraform FR1200 [29], the bulk density of the sintered part is $1.020\,g.cm^{-3}$. So, this high density indicates that the sintering process works well with this range of energy density.

The relative density of our specimens is in the range of 92–95%; it corresponds to a very low porosity rate of around 5–8%. The highest relative density of 95% was obtained for a fill energy density of $0.017\,J.mm^{-2}$ (exp. N°13). The highest porosity rate of 8% was achieved with a fill energy density of $0.015\,J.mm^{-2}$ (exp. N°38). In Figure 3, it can be seen that the porosity rate decreases, while the fill energy density increases. Ajoku et al. [13] have reported the density of the sintered sample of $0.96\,g.cm^{-3}$, while the density of injection moulded PA12 was measured at $1.03\,g.cm^{-3}$. In injection moulding, the porosity rate is usually very low due to the high pressure applied to the melted polymer when it is pushed into the mould. When comparing to injected specimens, a difference of 7% of porosity rate is measured for sintered parts.

3.1.2. Geometry and Dimensions. The dimensions of the printed parts are calculated by comparing the dimensions of the CAD models to the real dimensions of the printed parts.

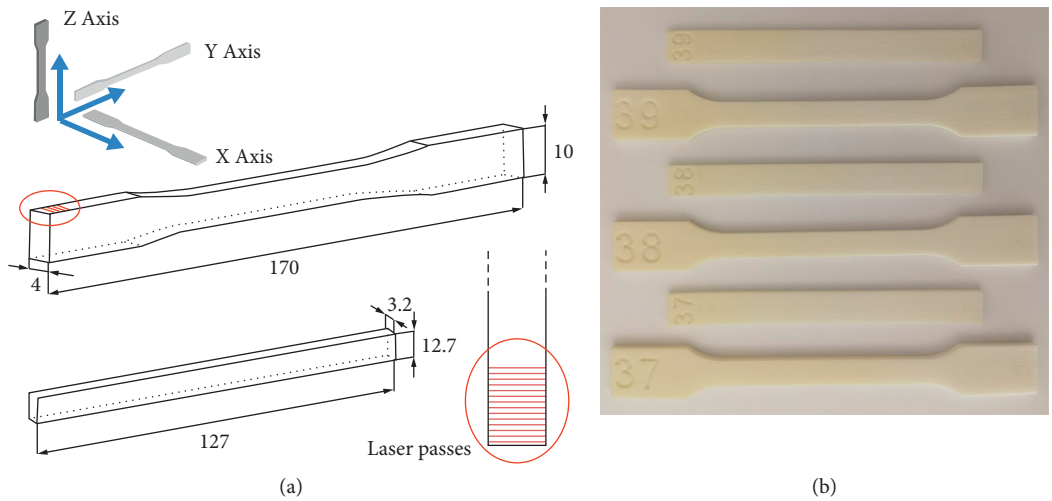

Figure 2: (a) Specimens design dimensions. (b) Printed specimens.

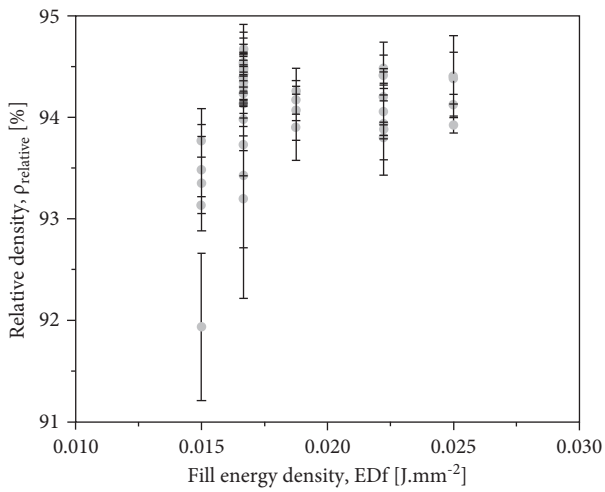

Figure 3: Effect of fill energy density on the relative density.

We target the minimum shrinkage since a high shrinkage leads to internal stress and part distortion. The thickness and width grow for all specimens, while their length decreases compared to the CAD model. The thickness and width are affected by the beam offset. Indeed, when the laser beam is absorbed by the polymer powder, the thermally affected zone is higher than the surface of the laser spot. As a result, the dimensions of the part are above the expected dimensions. The decrease in length can be attributed to shrinkage as the beam offset plays a minor role compared to the 170 mm of specimen's length. Indeed, when more energy is applied in a small area of thickness and width of samples, the specimens have a larger section (thickness x width). The higher growth is due to the scan spacing of 0.15 mm. The acceptable dimensional results (medium tolerance in length, thickness, and width for at least three samples), meaning low shrinkage, are seen in Figure 4 for exp. N°33 and N°38 for flexion and in Figure 5 for exp. N°38 and N°40 for tensile samples.

The shrinkage in the length and width is smaller than in the thickness of printed specimens. The high growth in the thickness shrinkage fluctuates in the range of −3% to −15% (exp. N°5) for the flexion samples and from −2% to −16% (exp. N°5) for the tensile samples. The max linear shrinkage is 0.4% in both length and width for tensile parts. In the case of flexion parts, the maximum linear shrinkage is 0.6% and 0.5% in length and width, respectively. Thus, the thickness depends on the outline scan count. For the outline scan count of two, the thickness shrinkage is lower.

The volume of flexion samples increases with the increase of fill energy density, as seen in Figure 6. This is due to high growth in the parts' thickness.

The shrinkage must be prevented as it implies the deformation of sintered parts. The distortion in SLS parts can be caused by stresses during the building and cooling processes [30]. The shrinkage is according to the type of materials, process parameters, and orientation of the sintered parts. The growth in part section may also occur because of thermal inhomogeneity within the powder bed.

3.1.3. Mechanical Properties. The stress-strain curves describe the typical yield behaviour of the material. The curves have been normalized to the maximal stress of each experiment. Strain-stress curves, as seen in Figure 7, are presented for exp. N°1, N°5, N°14, N°18, and N°27 corresponding to fill laser power of 15 W, 20 W, 30 W, 40 W, and 45 W, respectively.

The material behaviour is typical of polymeric specimens with a nonlinear curve. At first, the curve shows an elastic linear behaviour followed by a nonlinear viscoelastic behaviour. The curves have similar trends for all the tests performed; very little scatter is observed for different samples with the same set of parameters. Figure 7 shows a difference in mechanical response for tensile samples depending on the laser power. The effect of fill laser power on stress-strain curves of tensile specimens shows that increasing the laser power causes increasing in elastic modulus and elongation at break.

The viscoelastic behaviour of semicrystalline PA12 is associated with the deformation caused by straining the

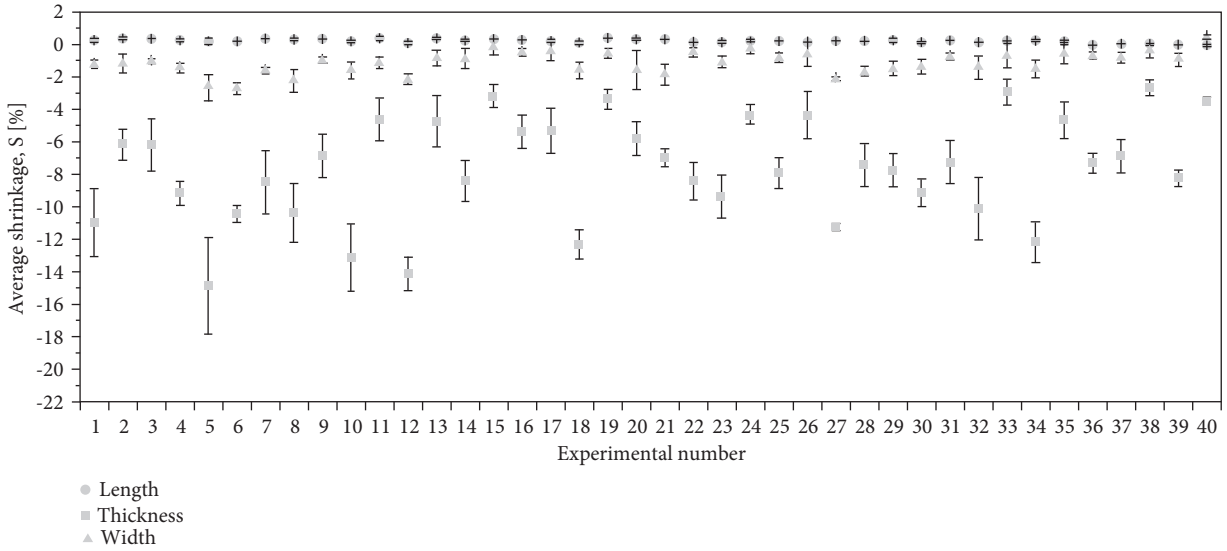

Figure 4: Average shrinkage of flexion samples.

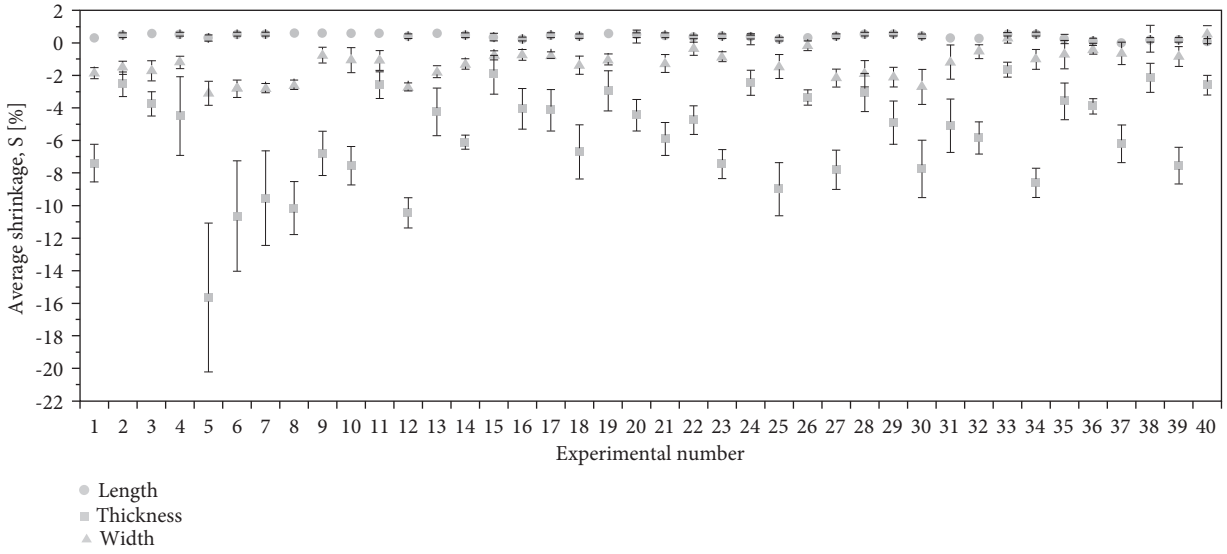

Figure 5: Average shrinkage of tensile samples.

interlamellar amorphous regions enclosed by crystallites. It can be said that a low degree of crystallinity may result in a low elastic modulus and a higher crystallinity in a higher modulus as the molecular chains are packed closely and parallel [17].

The mechanical properties of all sets of parameters do not reveal significant variations. The maximum flexural modulus and strength presented in Figure 8 are 1989 MPa for exp. N°3 and 68 MPa for exp. N°9, while the minimum values are 1764 MPa for exp. N°38 and 58 MPa for exp. N°38, respectively. The differences between the highest and the lowest values are 12% for flexural modulus and 14% for flexural strength obtained from normalization of the results to exp. N°9, as the results for a set of parameters proposed by the supplier. According to the datasheet of Duraform FR1200 [29], the flexural modulus and strength are 1770 MPa and 62 MPa, respectively. It means that higher values for flexural modulus and strength are obtained for almost all the SLS experiments.

The maximum and minimum elastic moduli presented in Figure 9 are 2142 MPa for exp. N°11 and 1888 MPa for exp. N°36, respectively. The values for tensile strength are at most 44 MPa for exp. N°3 and the lowest at 38 MPa for exp. N°36. Considering elongation at break, 5% has been found as the highest value for exp. N°31, while 3% is the lowest one for exp. N°33. The technical specification of Duraform FR1200 [29] indicates the elastic modulus of 2040 MPa and tensile strength of 41 MPa. Our results are close to these values. The elongation at break is lower than the value of 6% in the technical specification.

Considering another polyamide 12 (named PA2200), Wegner and Witt [9] found max values of 1758 MPa and

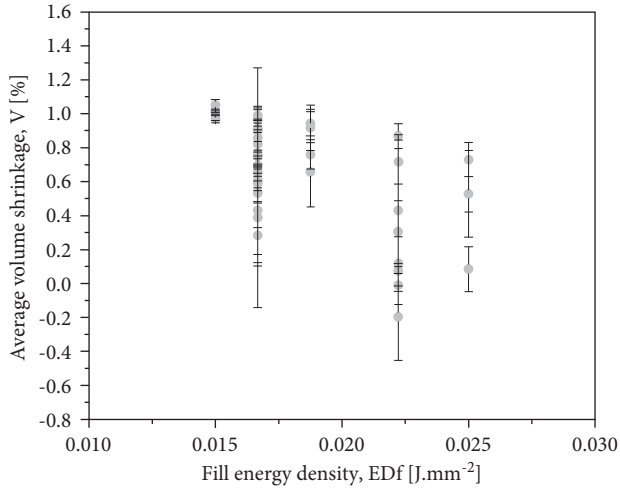

Figure 6: Effect of fill energy density on the average volume shrinkage of flexion samples.

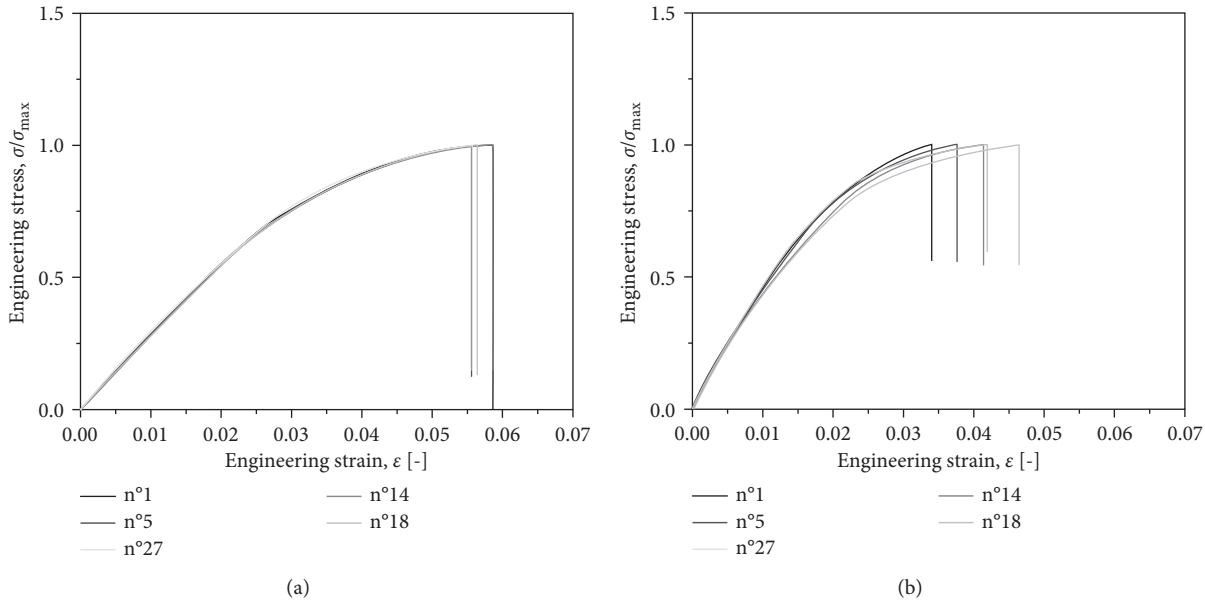

Figure 7: Normalized stress strain for (a) flexion samples and (b) tensile samples.

51 MPa (ED = 0.33 J.mm^{-3}) for elastic modulus and tensile strength, respectively. Still, with PA2200, Hofland et al. [14] have obtained the max of 2239 MPa (ED = 0.61 J.mm^{-3}) and 50.1 MPa (ED = 0.52 J.mm^{-3}), respectively. The values for elongation at break are 21% (Wegner and Witt) and 26% (Hofland et al.), which correspond to the value of 24% verified with the datasheet of material. Goodridge et al. [7] and Zarringhalam et al. [31] have reported that rapidly cooled products have a higher elongation at break than slowly cooled products. In addition to a difference in elongation at break, it is important to know that slow cooling results in higher crystallinity and more shrinkage [32].

The exp. N°11 and N°13 seem to offer the best mechanical properties by comparing flexural and tensile results (Figures 8 and 9). The flexural modulus and strength are 1957 MPa and 65 MPa, respectively. The elastic modulus, tensile strength, and elongation at break are 2118 MPa, 43 MPa, and 4%, respectively. It is worth noticing that even though some sets of parameters result in improved properties, the improvement is low (between 1 and 5%) compared to exp. N°9.

3.1.4. Thermal Transition. The thermal transitions and apparent crystallinity have been measured for all the specimens. The ranges of glass transition, crystallization, and melting temperatures vary around 10°C, 5°C, and 15°C of differences, respectively. The apparent crystallinity rate varies from 28.5% for exp. N°40 to 33.5% for exp. N°15. The uncertainty of measurement by differential scanning calorimeter is more or less 1%, while for the crystallinity rate, the accuracy is around 2%. The differences between experiments

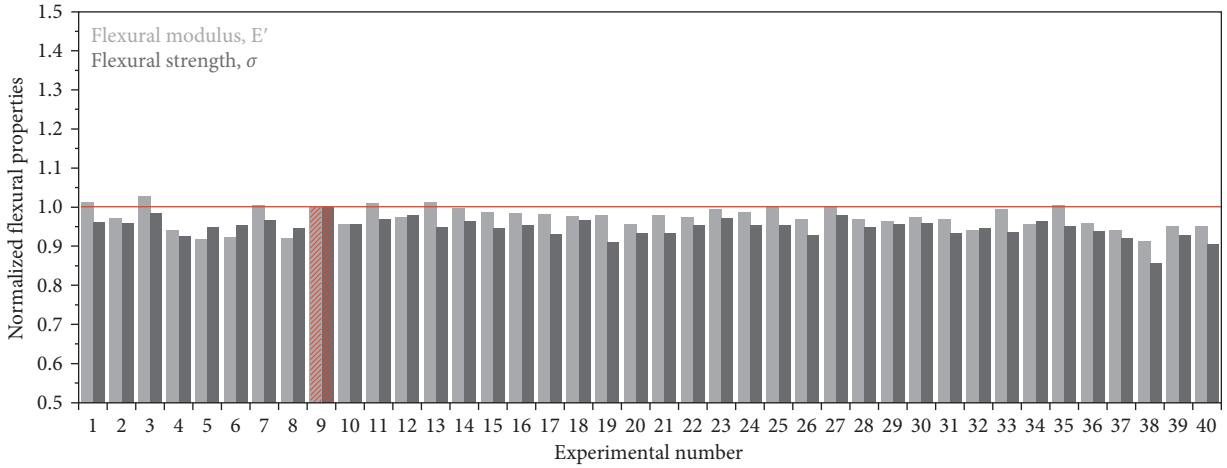

Figure 8: Normalized flexural properties of sintered parts compared to exp. N°9. The red line corresponds to exp. N°9, which represents the parameters recommended by the supplier.

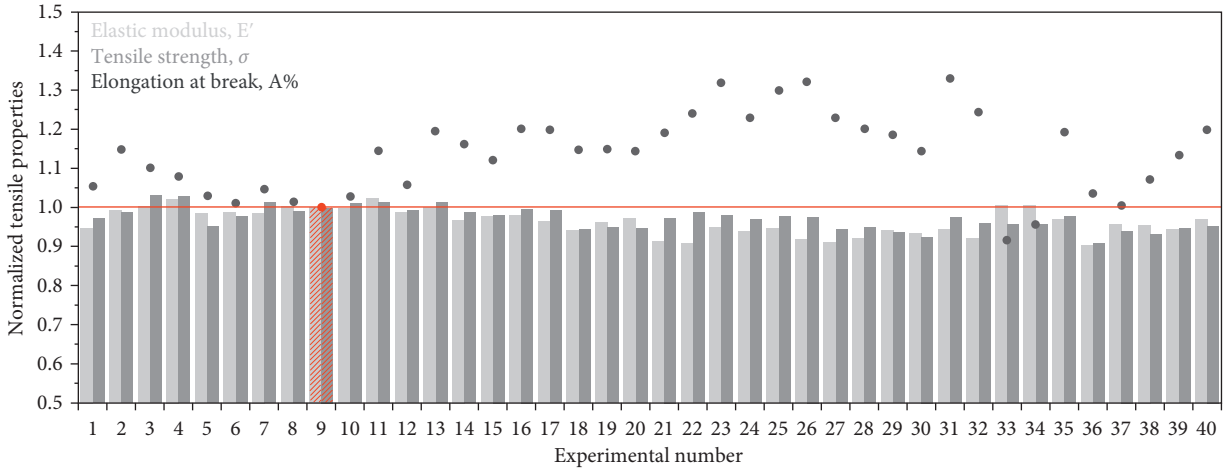

Figure 9: Normalized tensile properties of sintered parts compared to exp. N°9. The red line corresponds to exp. N°9, which represents the parameters recommended by the supplier.

stem from the various thermal history undergone by each specimen. We target the highest crystallinity rate since it signifies higher mechanical strength. The results are presented elsewhere [33], but they are included in the following statistical analysis to find correlations between process parameters and crystallinity.

3.1.5. Production Time. In Figure 10, the production time decreases from exp. N°1 to exp. N°40, while the fill laser power increases. Nevertheless, the production time is independent of the laser power, as seen in (5), but it depends on scan count and scan spacing.

The longest production time obtained is 91 s for exp. N°5 with LPf = 2 × 15 W, LPo = 2 × 10 W, and SS = 0.15 mm. The lowest one is 28 s for exp. N°40 with LPf = 1 × 45 W, LPo = 1 × 15 W, and SS = 0.25 mm. It can be noticed that the production time is higher with twice the scan count, which is caused by the double pass of the laser. Moreover, the higher scan spacing reduces the sintered area, so the production time is shorter. These results compared with the results of dimensional tolerances can draw the conclusion that the highest production time gives the best dimensions of samples.

3.2. Statistical Analysis

3.2.1. Global Sphere. A lighten approach with total data in Figure 11 illustrates the iconography of correlations diagram for 40 experiments and 26 variables: 5 studied parameters and 21 studied answers, presented in Table 3.

The threshold chosen for the lines representing remarkable correlations is 0.3. It is the default value used in the iconography of correlations. The link between two variables is named "remarkable" if this link subsists when any of the other variables are constant. For this global sphere, hydrostatic density and relative density are considered as variables correlated positively or negatively. Thus, this method removes relative density as the redundant variable. Moreover, links that are only due to one observation are not drawn.

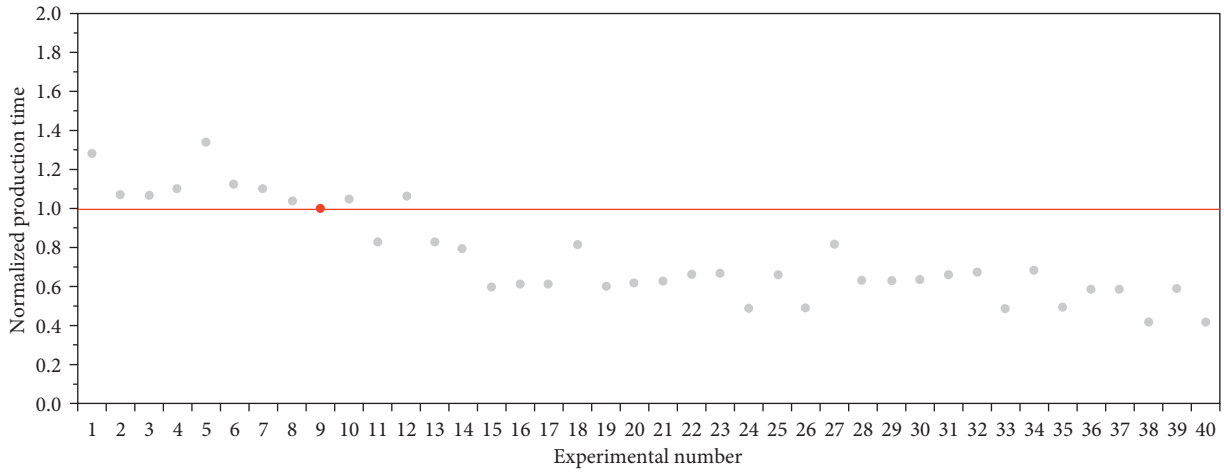

Figure 10: Normalized production time of flexural sintered parts compared to exp. N°9. The red line corresponds to exp. N°9, which represents the parameters recommended by the supplier.

Table 3: Variables during CORICO method.

Studied answers	LPf	Fill laser power
	SCf	Fill scan counting
	LPo	Outline laser power
	SCo	Outline scan counting
	SS	Scan spacing
Studied parameters	EDf	Fill energy density
	EDo	Outline energy density
	Dhyd	Hydrostatic density
	Drel	Relative density
	LSF	Flexural length shrinkage
	TSF	Flexural thickness shrinkage
	WSF	Flexural width shrinkage
	VSF	Flexural volume shrinkage
	LST	Tensile length shrinkage
	TST	Tensile thickness shrinkage
	WST	Tensile width shrinkage
	FlexuralM	Flexural modulus
	FlexuralS	Flexural strength
	TensileM	Tensile modulus
	TensileS	Tensile strength
	TensileE	Elongation at break
	Tp	Production time
	Tg	Glass transition temperature
	Tm	Melting point
	Tc	Crystallization temperature
	Xc	Apparent crystallinity

The geometric approach obtained from total data as a unique value produced by CORICO shows positive and negative correlations between variables. To give an example, the total correlations R^2, higher than 0.80, according to variables A and B, are presented in Table 4.

The obtained correlation can be justified. The best correlation of 0.92 is indicated for negative correlation, which comes from equation (7); the fill laser power (LPf) increases when the fill scan counting (SCf) decreases. Then, by considering positive correlations, when the fill scan spacing (LPf) passes more times, the production time (tp) is longer. From the calculation in equation (7), it is obvious that the outline energy density (EDo) increases when the outline scan counting (SCo) is higher because the laser passes more times with the same energy density at the same location.

Table 4: Positive and negative correlations of all the results.

A	B	R^2
LPf	−SCf	0.92
SCf	tp	0.88
SCo	EDo	0.80

3.2.2. Multiple Regression Models. The results of a global sphere and obtained correlations allow the calculation of the models of regression. The total correlations R^2 for energy density, mechanical properties, and production time, according to CORICO models for 5 regressors, are presented in Table 5.

The adjusted R^2 presents a total coefficient correlation. The best correlations are obtained for the fill energy density of 0.95, outline energy density of 0.99, and production time of 0.99. These values were directly calculated from the laser properties, so it confirms that the models are correct.

The several interactions obtained from models explain the most important interactions. The regressors involve nonlinear logical functions of factors, and the explanation is given as follows: the use of high laser power and short scan spacing has a strong influence on energy density (LP-SS). It means that a higher energy density is required. Strong influence on flexural properties is observed for two correlations with (a) medium outline laser power if low fill laser power (LPo{-LPf) and (b) high outline scan count while short scan spacing (SCo-SS). Moreover, low fill laser power and high scan count (LPf-SCf; SCf&SCo) influence tensile properties. The high fill scan count and short scan spacing (SCf&-SS) have a strong influence on production time.

The interactions of nonlinear logical functions can be demonstrated by three-dimension plots among the most significant process parameters for mechanical strength and production time, for example.

Table 5: Models of CORICO for 5 regressors.

EDf	$=1.9{\cdot}10^{-2} + 1.6{\cdot}10^{-2}$ LPf-SS + $1.5{\cdot}10^{-2}$ SCf}LPf + $7.8{\cdot}10^{-3}$ LPf&-SS
R^2	=0.95
EDo	$=4.0{\cdot}10^{-3} + 3.1{\cdot}10^{-2}$ LPo-SS + $1.7{\cdot}10^{-2}$ SCo + $6.0{\cdot}10^{-3}$ SCo}SS − $4.2{\cdot}10^{-3}$ SS&-LPo
R^2	=0.99
FlexuralM	= 1888.5 + 163.8 LPo{−LPf − 133.6 SCf-SCo + 131.3 LPo'SS + 97.6 LPf{-LPo
R^2	=0.22
FlexuralS	=64.7 + 7.7 SCo-SS
R^2	=0.31
TensileM	=1995.1 − 304.7 LPf{LPf − 137.9 SCo&-LPo
R^2	=0.42
TensileS	=40.9 − 7.5 LPf-SCf − 5.0 SCo-SS + 3.1 LPf!SS + 1.9 LPf#SS
R^2	=0.75
TensileE	= 4.1−1.1 SCf&SCo
R^2	= 0.12
Tp	=51.4 + 93.2 SCf&-SS + 41.6 SCo-SS + 17.6 SS]SCf + 6.3 SCf&SCo − 5.4 LPo'SS
R^2	=0.99

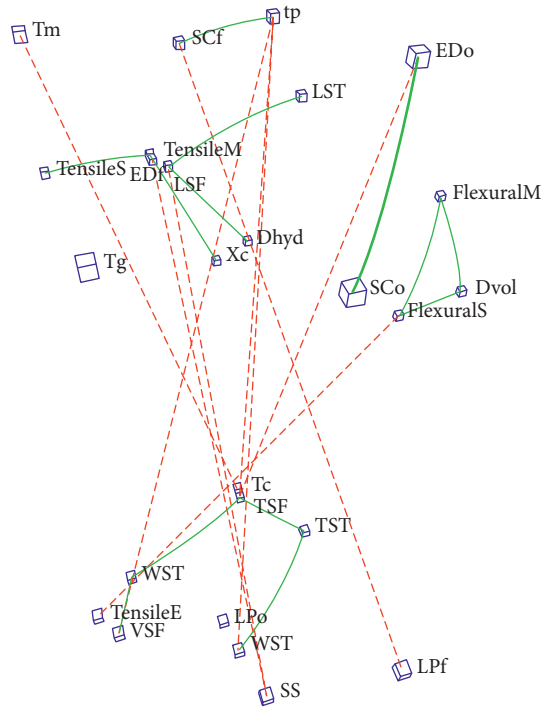

Figure 11: CORICO diagram of total results at threshold 0.3.

The flexural strength in Figure 12(a) shows significant interactions between outline scan count and scan spacing, while high values increase the flexural strength. This is because high flexural strength can be obtained by double outline scan count with shorter scan spacing. This is linked to high density, while more laser power on smaller areas causes a higher level of sintering. However, in Figure 12(b), the high tensile strength is caused by high fill laser power and low fill scan count or the opposite, meaning low fill laser power and high fill scan count. Moderate laser power is required instead of too high or too low impact of temperature.

The graph for production time in Figure 13 presents the interaction plots for fill scan count and scan spacing. With a high level of fill scan count and a short distance between laser passes, the production time is longer than for the specimen sintered at double fill scan count and high scan spacing. This can be explained by the fact that the part sintered with high scan spacing takes less time during printing. The production time is one of the most important parameters from the industrial point of view.

3.2.3. Optimization. The next step is to determine the optimal set of parameters in order to achieve desirable properties. The density and mechanical properties were maximized, while production time was minimized. It is expected that these goals may provide the best quality of printed parts as functional parts. The responses independent of the process were averaged to decrease its impact. The optimization criteria for obtaining a suitable set of parameters and the results are summarized in Table 6.

The optimal processing parameters to maximize density and mechanical properties while minimizing production time rounded off are as follows: fill laser power of 28.2 W, fill scan count of 1 (1.17), outline laser power of 15 W, outline scan count of 1, and scan spacing of 0.16, which is in reasonable agreement with predicted responses. For these parameters, the fill energy density is 0.017 J.mm$^{-2,}$ and for the outline, the energy density is 0.027 J.mm^{-2}. The predicted mechanical properties for these set of parameters show a slight increase of tensile strength, tensile modulus, flexural strength, and flexural modulus of 42 MPa, 2042 MPa, 64 MPa, and 1868 MPa, as compared to the values in the technical specification for Duraform FR1200 [29] of 41 MPa, 2040 MPa, 62 MPa, and 1770 MPa, respectively. In the case of elongation at break, it decreases from 6% to 4%. The production time is estimated at 45 s, which is half the maximum time calculated to print one sample following the exp. N°5 (91 s). The saving time is the difference between recommended parameters and the ones we have defined. The production time for recommended processing parameters is 68 s, while for optimal processing parameters, it is 45 s.

The recommended processing parameters are represented by the exp. N°9, which corresponds to fill laser power of 2 × 20 W, outline laser power of 2 × 10 W, and

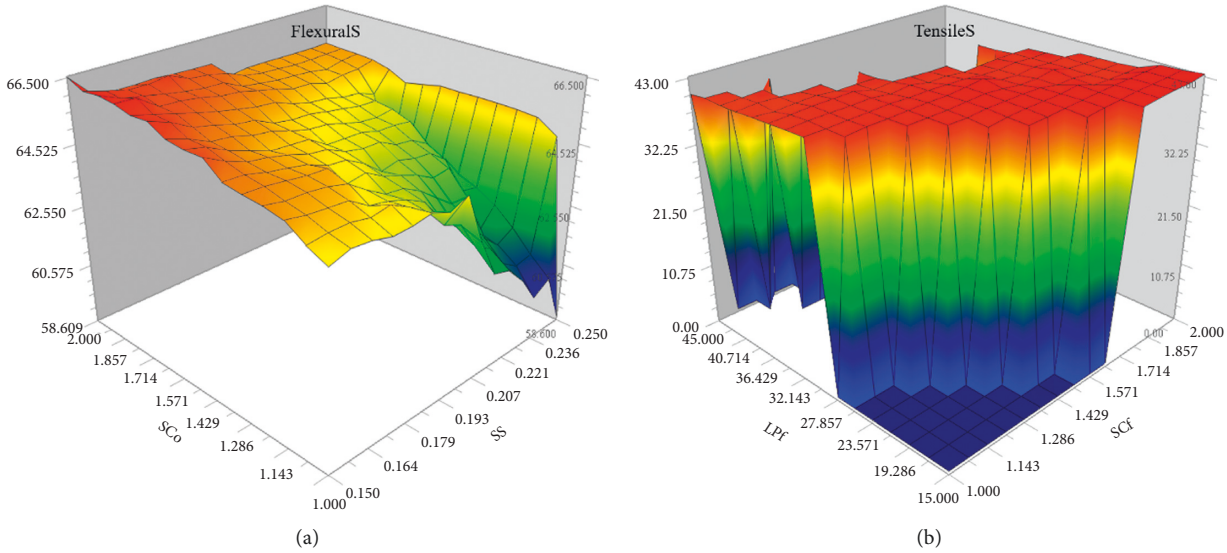

Figure 12: The 3D response surface plots for (a) flexural and (b) tensile strength.

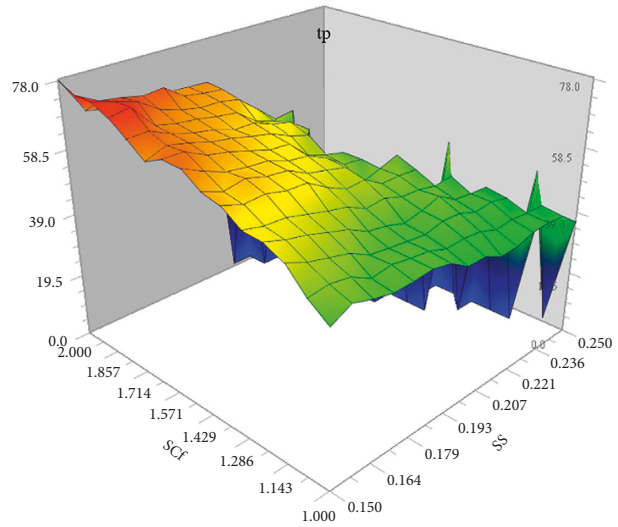

Figure 13: The 3D response surface plots for production time.

Table 6: Proposed optimization criterion with results.

Conditions and response	Minimum	Maximum	Results	Unit
LPf	15.00	45.00	28.20	W
SCf	1.00	2.00	1.17	—
LPo	10.00	15.00	15.00	W
SCo	1.00	2.00	1.00	—
SS	0.15	0.25	0.16	mm

scan spacing of 0.20 mm proposed by the supplier of machine and powder (3D Systems), and the production time is estimated for 68 s. Looking deeper at the experiments, the exp. N°17 is the closest one to the defined optimal set. The experiment corresponds to fill laser power of 1×30 W, outline laser power of 1×15 W, and scan spacing of 0.15 mm. So, the best properties are supposed to be achieved with the set of parameters. To remember, the flexural modulus is 1897 MPa, the flexural strength is 64 MPa, the elastic modulus is 2015 MPa, the tensile strength is 42 MPa, the elongation at break is 4.2%, and the production time is 41 s.

4. Conclusions

In this work, 400 samples were produced by SLS with 40 different sets of parameters using a commercial machine ProX500 SLS. The material is polyamide 12 powder. The energy density range is between 0.015 J.mm^{-2} and 0.043 J.mm^{-2}.

The specimens were characterized to measure their density and mechanical properties. The results of the characterization of specimens show that the chosen parameters are suitable to successfully produce printed parts at various laser power. A low porosity rate at a maximum of 8% is measured for the printed samples with a density in the range between 0.97 g.cm^{-3} and 1.04 g.cm^{-3}. The small shrinkage in the length and width was evident. The volume of sintered parts increases with the increase of energy density due to the growth in the thickness of the part. The mechanical properties and production time are compared to the set of parameters N°9, proposed by the machine and powder supplier. We achieve better properties by changing some parameters, for instance, in the exp. N°11 and N°13. The highest flexural modulus and strength values obtained are 1989 MPa and 68 MPa, respectively. Elastic modulus, tensile strength, and elongation at break are 2142 MPa, 44 MPa, and 5% at most, respectively. The production time decreases with an increase in laser power and a decrease in scan count. The thermal properties and crystalline rate do not show significant variations.

The optimization of the process parameters was done by the iconography of correlations method. The design of experiments was based on laser power, scan count, and scan spacing for both fill and outline regions of the parts.

The optimization of the laser parameters shows how the production time is influenced. The double fill scan count and short scan spacing have a strong influence. It is obvious that increasing the distance between successive laser beam passes allows for a significant reduction in manufacturing time. However, in our optimization, we suggest using one fill scan count and decreasing the distance between successive laser beam passes by simultaneously obtaining better properties of printed samples. It is observed at the same time a slight increase in the porosity of the material. The mechanical properties are more affected by laser power and scan count. The main reason behind this is that when sintering takes place at high laser power, the adhesion between the powder particles becomes stronger, increasing the density, modulus, and strength of the printed specimens. Moreover, the flexural properties can be improved with a double scan count. The tensile properties require a double fill scan count and one pass of outline laser power to reach better properties. This might be because when the scan count increases, the energy absorbed by the material at a unit time and a unit area increases, which leads to better melting by energy delivered to the powder bed. Hence, by optimizing the laser parameters, it is possible to obtain the targeted mechanical properties with over 33% production time savings. Consequently, the manufacturing cost of printed parts could be reduced.

This work illustrates that the iconography of correlations is an effective tool to optimize the properties of printed parts and the manufacturing cycle. This study was carried out with polyamide 12, but the same methodology used in this paper is applicable to any other materials as far as they are suitable for the SLS process. Simultaneously, other SLS machines equipped with fill and outline scanning strategies can be adapted.

Data Availability

The input data of CORICO used to support the findings of this study are available from the corresponding author upon request.

Conflicts of Interest

The authors declare that they have noconflicts of interest.

Acknowledgments

This work received financial support from ANRT through a CIFRE Ph.D. fellowship (Grant no. 2016/0236) and from the Occitanie region through a Pile-CIFRE contract and by the company Prismadd Additive Manufacturing, part of the WeAre group.

References

[1] L. Lü, J. Y. H. Fuh, and Y. S. Wong, *Laser-induced Materials and Processes for Rapid Prototyping*, Springer Science & Business Media, New York, NY, USA, 2013.

[2] N. Kumar, H. Kumar, and J. S. Khurmi, "Experimental investigation of process parameters for rapid prototyping technique (selective laser sintering) to enhance the part quality of prototype by Taguchi method," *Procedia Technology*, vol. 23, no. 1, pp. 352–360, 2016.

[3] G. Guan, M. Hirsch, Z. H. Lu et al., "Evaluation of selective laser sintering processes by optical coherence tomography," *Materials & Design*, vol. 88, no. 1, pp. 837–846, 2015.

[4] S. Berretta, K. E. Evans, and O. Ghita, "Processability of PEEK, a new polymer for high temperature laser sintering (HT-LS)," *European Polymer Journal*, vol. 68, no. 1, pp. 243–266, 2015.

[5] T. Gill and B. Hon, "Selective laser sintering of SiC/polyamide composites," *CIRP Annals*, vol. 52, no. 1, pp. 173–176, 2003.

[6] B. Caulfield, P. E. McHugh, and S. Lohfeld, "Dependence of mechanical properties of polyamide components on build parameters in the SLS process," *Journal of Materials Processing Technology*, vol. 182, no. 1–3, pp. 477–488, 2007.

[7] R. D. Goodridge, C. J. Tuck, and R. J. M. Hague, "Laser sintering of polyamides and other polymers," *Progress in Materials Science*, vol. 57, no. 2, pp. 229–267, 2012.

[8] Y. Khalil, A. Kowalski, and N. Hopkinson, "Influence of energy density on flexural properties of laser-sintered UHMWPE," *Additive Manufacturing*, vol. 10, no. 1, pp. 67–75, 2016.

[9] A. Wegner and G. Witt, "Correlation of process parameters and part properties in laser sintering using response surface modeling," *Physics Procedia*, vol. 39, no. 1, pp. 480–490, 2012.

[10] S. Negi, S. Dhiman, and R. K. Sharma, "Determining the effect of sintering conditions on mechanical properties of laser sintered glass filled polyamide parts using RSM," *Measurement*, vol. 68, no. 1, pp. 205–218, 2015.

[11] A. E. Tontowi and T. H. C. Childs, "Density prediction of crystalline polymer sintered parts at various powder bed temperatures," *Rapid Prototyping Journal*, vol. 7, no. 3, pp. 180–184, 2001.

[12] S. Griessbach, R. Lach, and W. Grellmann, "Structure-property correlations of laser sintered nylon 12 for dynamic dye testing of plastic parts," *Polymer Testing*, vol. 29, no. 8, pp. 1026–1030, 2010.

[13] U. Ajoku, N. Hopkinson, and M. Caine, "Experimental measurement and finite element modelling of the compressive properties of laser sintered nylon-12," *Materials Science and Engineering*, vol. 428, no. 1–2, pp. 211–216, 2006.

[14] E. C. Hofland, I. Baran, and D. A. Wismeijer, "Correlation of process parameters with mechanical properties of laser sintered PA12 parts," *Advances in Materials Science and Engineering*, vol. 2017, no. 1, pp. 1–11, 2017.

[15] W. A. Y. Yusoff and A. J. Thomas, "The effect of employing an effective laser sintering scanning strategy and energy density value on eliminating "orange peel" on a selective laser sintering part," in *Proceedings of the 17th International Association for Management of Technology*, pp. 1–16, Dubai, 2008.

[16] A. Stwora and G. Skrabalak, "Influence of selected parameters of selective laser sintering process on properties of sintered materials," *Journal of Achievements in Materials and Manufacturing Engineering*, vol. 61, no. 2, pp. 375–380, 2013.

[17] F. Shen, S. Yuan, C. K. Chua, and K. Zhou, "Development of process efficiency maps for selective laser sintering of polymeric composite powders: modeling and experimental testing," *Journal of Materials Processing Technology*, vol. 254, no. 1, pp. 52–59, 2018.

[18] A. Korycki, C. Garnier, N. Rodier, F. Chabert, E. Laurent, and V. Nassiet, "Numerical and experimental analysis of the thermal profile of printed layers during selective laser sintering process of poly(etheretherketone)," in *Proceedings of the 22nd International ESAFORM Conference on Material Forming*, p. 150005, Vitoria-Gasteiz, Spain, 2019.

[19] S. Yuan, J. Bai, C. Chua, J. Wei, and K. Zhou, "Material evaluation and process optimization of CNT-coated polymer powders for selective laser sintering," *Polymers*, vol. 8, no. 10, p. 370, 2016.

[20] S. A. Aldahash, S. A. Salman, and A. M. Gadelmoula, "Towards selective laser sintering of objects with customized mechanical properties based on ANFIS predictions," *Journal of Mechanical Science and Technology*, vol. 34, no. 12, pp. 5075–5084, 2020.

[21] P. Dardenne and J. A. Fernández Pierna, "A NIR data set is the object of a chemometric contest at "Chimiométrie 2004"," *Chemometrics and Intelligent Laboratory Systems*, vol. 80, no. 2, pp. 236–242, 2006.

[22] C. Lesty, J. Pleau-Varet, and M. Kujas, "Geometric method and generalized linear models. Two opposite multiparametric approaches illustrated on a sample of pituitary adenomas," *Journal of Applied Statistics*, vol. 31, no. 2, pp. 191–213, 2004.

[23] J.-C. Lee and S.-H. Ahn, "Bulk density measurement of porous functionally graded materials," *International Journal of Precision Engineering and Manufacturing*, vol. 19, no. 1, pp. 31–37, 2018.

[24] S. Gogolewski, K. Czerntawska, and M. Gastorek, "Effect of annealing on thermal properties and crystalline structure of polyamides. Nylon 12 (polylaurolactam)," *Colloid & Polymer Science*, vol. 258, no. 10, pp. 1130–1136, 1980.

[25] M. Lesty, "La recherche des harmoniques une nouvelle fonction du logiciel CORICO," *Revue Modulad*, vol. 29, no. 1, pp. 34–74, 2002.

[26] I. Gibson and D. Shi, "Material properties and fabrication parameters in selective laser sintering process," *Rapid Prototyping Journal*, vol. 3, no. 4, pp. 129–136, 1997.

[27] J. S. Usher, T. J. Gornet, and T. L. Starr, "Weibull growth modeling of laser-sintered nylon 12," *Rapid Prototyping Journal*, vol. 19, no. 4, pp. 300–306, 2013.

[28] S. Dupin, O. Lame, C. Barrès, and J.-Y. Charmeau, "Microstructural origin of physical and mechanical properties of polyamide 12 processed by laser sintering," *European Polymer Journal*, vol. 48, no. 9, pp. 1611–1621, 2012.

[29] "3D Systems," *Datasheet of Duraform FR1200*, https://www.3dsystems.com/sites/default/files/2018-03/3d-systems-duraform-fr1200-datasheet-usen-2018-03-20-web.pdf, 2018.

[30] K. Manetsberger, J. Shen, and J. Muellers, "Compensation of non-linear shrinkage of polymer materials in selective laser sintering," in *Proceedings of the Solid Freeform Fabrication Symposium*, pp. 346–356, Austin, TX, USA, 2001.

[31] H. Zarringhalam, N. Hopkinson, N. F. Kamperman, and J. J. de Vlieger, "Effects of processing on microstructure and properties of SLS nylon 12," *Materials Science and Engineering*, vol. 435-436, no. 1, pp. 172–180, 2006.

[32] Y. Shi, Z. Li, H. Sun, S. Huang, and F. Zeng, "Effect of the properties of the polymer materials on the quality of selective laser sintering parts," *Proceedings of the Institution of Mechanical Engineers-Part L: Journal of Materials: Design and Applications*, vol. 218, no. 3, pp. 247–252, 2004.

[33] A. Korycki, *Study of the Selective Laser Sintering Process: Materials Properties and Effect of Process Parameters*, Doctorat Dissertations, Université de Toulouse, 2020.